On the compositional variability of dalyite, $K_2ZrSi_6O_{15}$: a new occurrence from Terceira, Azores

A. J. Jeffery[a*], R. Gertisser[a], R. A. Jackson[a], B. O'Driscoll[a, b], A. Kronz[c]

a) *School of Physical and Geographical Sciences, Keele University, Keele, Staffordshire, ST5 5BG, United Kingdom*

b) *School of Earth, Atmospheric and Environmental Sciences, The University of Manchester, Oxford Road, Manchester, M13 9PL*

c) *Geowissenschaftliches Zentrum Göttingen, Goldschmidtstrasse 3, D-37077 Göttingen, Germany*

* Corresponding author:

Tel. +44 (0) 1782 733620

E-mail *a.j.jeffery@keele.ac.uk*

Running title: A new occurrence of dalyite, Azores

Abstract

The rare potassium zirconium silicate dalyite has been identified for the first time on Terceira, Azores, within syenitic ejecta of the Caldeira-Castelinho Ignimbrite Formation. New quantitative analyses of this dalyite are combined with the small number of published analyses from various locations worldwide to evaluate the mineral's compositional variability. Additionally, solid-state modelling has been applied to assess the site allocations of substituting elements. The new analyses yield the average formula $(K_{1.84}Na_{0.15})_{\sum=1.99}(Zr_{0.94}Ti_{0.012}Hf_{0.011}Fe_{0.004})_{\sum=0.967}Si_{6.03}O_{15.}$ Model results predict the placement of substituting Hf and Ti in the octahedral site, and highlight the overall difficulty in the incorporation of Fe, Mg and Ba. The combined dataset reveals that dalyite found within peralkaline granites and syenites is generally defined by higher Na↔K substitution and lower Ti↔Zr substitution relative to dalyite from highly potassic rocks. The Terceira dalyite exhibits a bimodal variation in the degree of Na↔K substitution which is attributed to a K-enrichment trend induced by late stage pore wall crystallisation and albitization, coupled with the control of pore size upon the degree of supersaturation required to initiate nucleation of dalyite in pores of varying size.

Key words: Dalyite, Peralkaline, Syenite, Oceanic island magmatism, Terceira, Azores

Introduction

Dalyite is a rare potassium zirconium silicate, with the empirical formula $K_2ZrSi_6O_{15}$. It was first identified in peralkaline granitic ejecta found within the pyroclastic sequences of Green Mountain and Middleton Peak, Ascension Island (Van Tassel, 1952). Since its discovery, it has been identified as an accessory phase in a variety of rocks, including peralkaline granites and syenites, late-stage pegmatites, charoitites, lamproites, lamprophyres, fenites and carbonatites (e.g. Furnes et al., 1982; Robins et al., 1983; Harris & Rickard, 1987; Linthout et al., 1988; Konev et

al., 1996). Having been established as a general indicator of peralkaline conditions, silica-oversaturation, and high chemical potential of K_2O (μK_2O) (e.g. Marks et al., 2011), the presence and composition of dalyite may provide important insights into the evolution of these magmatic systems.

Here, we report the first known occurrence of dalyite from the mildly peralkaline rocks of Terceira, Azores. We apply solid-state modelling to investigate various proposed substituting elements, and complement the existing global database with new high quality quantitative chemical analyses of dalyite from Terceira. Using these analyses, alongside whole rock major element analyses of the host syenites, we discuss the geochemical variability of dalyite, based on previously published compositions from both similar and contrasting rock types.

Background

Dalyite occurrences

Following the initial discovery of dalyite (Van Tassel, 1952), it was next identified in peralkaline syenitic ejecta from Agua de Pau volcano, São Miguel, Azores (Cann, 1967; Widom et al., 1993); where it was observed as an entirely intercumulus phase and therefore inferred by Ridolfi et al. (2003) to be the last mineral to crystallise (alongside quartz). Lazebnik & Makhotko (1982) identified dalyite in the Murun Complex, Siberia, Russia, also providing additional quantitative analyses. Furnes et al. (1982) and Robins et al. (1983) noted the presence of dalyite within a highly potassic lamprophyric dyke in Sunnfjord, Norway. Raade & Mladeck (1983) reported dalyite within a peralkaline granite pluton at Gjerdingen, Norway, where it was typically found in close contact with janhaugite $Na_3Mn_3Ti_2Si_4O_{15}(OH,F,O)_3$. Harris and Rickard (1987) recorded the occurrence of dalyite, alongside eudialyte, in a peralkaline granitic dyke that cross-cuts the nepheline syenites of the Straumsvola Complex, Antarctica. In 1988, an enstatite-sanidine-phlogopite lamproite in south-eastern Spain was reported to contain the mineral's first known occurrence in an extrusive rock (Venturelli et al., 1984; Linthout et al., 1988). Soon afterwards, dalyite was observed within fenites from the Serra Negra and Salitre – carbonatite alkaline igneous complex, Brazil (Mariano & Francis, 1989; Mariano &

Marchetto, 1991; Brod, 1999). Dalyite was later identified in the Strange Lake peralkaline granite complex, Canada, and noted to have nucleated heterogeneously onto older zircon crystals (Birkett et al., 1992; Salvi & Williams-Jones, 1995). Subsequent reported occurrences include the Amis peralkaline granite intrusion of the Brandberg Complex, Namibia (Schmitt et al., 2000), the various lithologies of the Murun Complex, Siberia, Russia (e.g. Dolivo-Dobrovol'skiy & Yevdokimov, 1991; Konev et al., 1996; Reguir, 2001), the Gordon Butte pegmatites, Montana, USA (Chakhmouradian & Mitchell, 2002), peralkaline granite dykes to the north of the Zargat Na'am ring complex, Egypt (Saleh, 2006), more unusually, a nepheline-bearing pegmatite, Langesundfjord, Norway (Andersen et al., 2010) and the alkali syenites and metasomatites of the Shibanovsky Massif, Russia (Stepnova et al., 2013) (Fig. 1).

The occurrence documented here is within quartz syenite ejecta sampled from the Caldeira-Castelinho Ignimbrite Formation (CCI) on Terceira Island, Azores (Gertisser et al., 2010). The nine Azorean islands straddle the Mid-Atlantic Ridge in the central North Atlantic Ocean and mark a triple junction between the American, Eurasian and African plates (e.g. Krause & Watkins, 1970). All nine islands are volcanic in origin and represent the subaerial manifestation of a large submarine plateau, itself interpreted to have originated from the interaction of a mantle plume with the Mid-Atlantic Ridge (e.g. Gente et al., 2003). The CCI is one of at least seven ignimbrite formations found within the stratigraphy of Terceira (Self, 1974, 1976; Gertisser et al., 2010) and can be readily distinguished from its counterparts by its relative abundance of quartz syenite ejecta (Gertisser et al., 2010). The discovery of dalyite within these ejecta marks the mineral's second known occurrence within the Azores archipelago.

Mineral properties

Van Tassel (1952) provided the first description of the physical properties, chemical composition, unit cell and x-ray powder diffraction data of dalyite. It is a triclinic, colourless mineral of moderate positive relief, exhibiting up to second order interference colours. The unit cell was defined as $K_2ZrSi_6O_{15}$, though the potential

substitutions of Na for K, and Hf for Zr, were suggested. The chemical similarity between dalyite and wadeite ($K_2ZrSi_3O_9$) was also noted. The original quantitative chemical analysis of dalyite is reported in Table 1 (analysis 1).

The crystal structure of dalyite was determined by Fleet (1965), who defined it as a phyllosilicate comprising four-, six- and eight-membered rings of SiO_4 tetrahedra. These sheets are linked by regular ZrO_6 octahedra and irregular $(K,Na)O_8$ polyhedra. Robins et al. (1983) provided 10 quantitative chemical analyses of dalyite from Sunnfjord, Norway and presented evidence for the substitution of Zr with Ti, and K with Fe, suggesting the more accurate empirical formula $(K,Na,Fe)_2(Zr,Ti)Si_6O_{15}$. They also highlighted the compositional similarity between dalyite and darapiosite, $KNa_2LiMnZnZrSi_{12}O_{30}$, sogdianite, $(K,Na)_2Li_2(Li,Fe,Al,Ti)_2Zr_2(Si_2O_5)_6$ and zektzerite, $LiNaZrSi_6O_{15}$. Further chemical analyses of dalyite were reported by Harris et al. (1982), Lazebnik & Makhotko (1982), Harris & Rickard (1987), Linthout et al. (1988), Birkett et al. (1992), Konev et al. (1996), Reguir (2001), Chakhmouradian & Mitchell (2002) and Ridolfi et al. (2003) (Table 1).

Methods

Analytical procedure

Whole rock major element analyses of the syenite ejecta were undertaken at Acme Analytical Laboratories Ltd, Canada, using x-ray fluorescence (XRF) spectrometry (samples TER 30-1, TER 30-6, TER35-1), and inductively coupled plasma atomic emission spectroscopy (ICP-AES) (TER 30-7). Weathered surfaces were removed and samples were crushed in an agate mill, prior to drying for 2 hours at 110 °C and a $LiBO_2$ fusion. Loss-on-ignition (LOI) was reported as the weight difference after ignition for 2 hours at 1,000 °C.

Semi-quantitative analyses and element maps were produced using a Hitachi TM-3000 scanning electron microscope (SEM) equipped with a Bruker Quantax 70 energy dispersive system (EDS) at Keele University, U.K. Quantitative major element analyses of dalyite were achieved for samples TER 30-1 and TER

30-7 using a JEOL JXA 8900 RL electron microprobe at the Georg-August Universität Göttingen, Germany. Peak counting times were 15 seconds for Si, Ti, Al, Fe, Mg, Ca, Na and K, and 30 seconds for Cr, Zr, Hf, Mn and Ba, using an acceleration voltage of 15 kV, a beam current of 15 nA and a 20 µm defocused beam. The following natural silicate minerals and synthetic materials (denoted as formulae) were used as primary standards: olivine (Si, Mg), albite (Na), sanidine (K), TiO_2 (Ti), haematite (Fe), anorthite (Al), wollastonite (Ca), Cr_2O_3 (Cr), rhodonite (Mn), celsian (Ba), $ZrSiO_4$ (Zr) and $HfSiO_4$ (Hf). Detection limits and errors (Table 2) were calculated at a confidence level of two-sigma from the raw background noise and the signal/background counting, respectively, following the Gaussian law of error propagation. The intensities were converted into concentrations by taking the matrix corrections into account.

Solid state modelling

Solid state modelling calculations were carried out to investigate the substitution of a number of potential substituting cations (Ti, Hf, Fe, Ba and Mg). This was undertaken using the GULP code (Gale, 1997). This code uses effective interatomic potentials to model the interactions between atoms, and has been widely used to calculate the structure and properties of inorganic materials. The Buckingham potential, supplemented by an electrostatic term, is used:

$$V(r) = A \exp(-r/\rho) - Cr^{-6} + q_1 q_2 / r$$

In this equation, the parameters A, ρ and C are fitted to structures and properties of related materials; here they have been transferred from studies on zircon (Akhtar & Waseem, 2001). The charges of the interacting ions are q_1 and q_2. The experimental and calculated lattice parameters for dalyite are given in Table 3 below, using the experimental structure from Fleet (1965) for comparison. It is seen that the lattice parameters agree to within a few percent, which gives confidence in using this transferred potential. The calculations reported here have been used to obtain the energies involved when various ions are substituted into the dalyite

lattice. The calculation of substitutional and solution energies for dopant ions in materials has been widely described elsewhere; see, for example, a recent study of Nd, Gd and Yb ions in BaF_2 (Mujaji et al., 2014). However, a brief summary will be given here. In the case of the substitution of Ti^{4+} into the dalyite lattice, the following reaction (solution scheme) is considered, assuming substitution at the Zr^{4+} site:

$$TiO_2 + Zr_{Zr} \rightarrow Ti_{Zr} + ZrO_2$$

The energy of this reaction (the solution energy), E_{sol}, is then calculated, as follows:

$$E_{sol} = [E_{latt}(ZrO_2) + E(Ti_{Zr})] - E_{latt}(TiO_2)$$

In this case no charge compensation is needed, but considering substitution at the K^+ site, the following scheme was assumed (with charge compensation by K^+ vacancies):

$$TiO_2 + 4K_K \rightarrow Ti_K^{\bullet\bullet\bullet} + 3V_K' + 2K_2O$$

The solution energy for this reaction is:

$$E_{sol} = [E(Ti_K^{\bullet\bullet\bullet}) + 3E(V_K') + 2E_{latt}(K_2O)] - E_{latt}(TiO_2)$$

In each case, a similar procedure is adopted, and a single solution scheme is assumed. More complex solution schemes, such as coupled substitutions, cannot be ruled out. Note that in the above expressions, Kröger-Vink notation has been used (Kröger & Vink, 1956).

Results

Petrography of the Caldeira-Castelinho Ignimbrite ejecta

Mineral assemblages of the CCI syenite ejecta include sodic alkali-feldspar, Na-pyroxene, Na-Ca to Na amphibole, quartz, aenigmatite and fayalite with accessory

Ti-magnetite, ilmenite, apatite, dalyite, an unspecified eudialyte group phase and biotite. Significant grain-size variation exists between nodules, allowing the broad distinction of two groups; fine to medium (~ 0.5 to 1.5 mm) grained nodules (Fig. 2a), and medium to coarse (~ 1.0 to 6.0 mm) grained nodules (Fig. 2b). Typically, the fresher samples are more friable, whereas the more altered samples appear more indurated. Some samples exhibit patches of granular texture, comprising predominantly alkali-feldspar and quartz of finer grain size than the surrounding material. Rarely, samples exhibit mineral modal and/or grain size layering at the cm-scale.

Alkali-feldspar is by far the most abundant phase in all of the nodules and ranges from fresh and unaltered crystals, to heavily altered, perthitic crystals. Pyroxenes and amphiboles are the dominant intercumulus phases. Quartz is also an intercumulus phase and is generally found as large rounded grains or aggregates. Aenigmatite is typically present in small amounts and often exhibits a complex reaction relationship with pyroxene, amphibole and Fe-Ti oxides. When not associated with the apparent breakdown of aenigmatite, Fe-Ti oxides are usually observed as inclusions within other phases (primarily alkali-feldspar). Apatite exists as small, acicular inclusions within alkali-feldspars and varies in abundance between samples. Dalyite is typically present as small (< 0.5 mm) sub- to anhedral crystals (Fig. 2c-e), though can reach sizes of 1 to 1.5 mm (Fig. 2f). It is almost exclusively anhedral and confined to the interstices, either filling or partially filling void spaces. It is often associated spatially with quartz, and in some cases can be found as inclusions within larger interstitial quartz crystals. An unspecified eudialyte-group mineral is rarely found as frequently zoned anhedral crystals that, like dalyite, appear to totally or partially infill interstitial pore spaces, and are often spatially associated with clinopyroxene. Biotite is uncommon and, where present, exists as small inclusions within alkali-feldspars.

Whole rock and mineral compositions

Whole rock

Four whole rock major element analyses of dalyite-bearing syenite nodules are given in Table 4. Major element compositions are relatively uniform between samples, with the variation of individual elements generally being restricted to less than 1 wt. %. Peralkalinity indices and Na_2O/K_2O ratios range from 1.08 to 1.14 and 1.42 to 1.51, respectively. Calculated CIPW norms yield quartz, albite, orthoclase, diopside, hypersthene, acmite, ilmenite, apatite and sodium metasilicate. All samples are silica-oversaturated, with between 1.0 and 3.3 wt. % normative quartz.

Dalyite chemistry

New chemical analyses of the CCI syenite dalyite (samples TER 30-1 and TER 30-7) are reported in Table 5. The data reveal that the CCI syenite dalyite does not deviate substantially from the empirical formula, with Na being the most significant substituting element (~ 0.10 to 0.20 apfu), substituting for K. The combined totals of atomic Na and K are close to the ideal total of 2 cations, and Fe contents are often below detection limit (0.038 wt. %, average error = 0.052 wt. %), highlighting limited incorporation of Fe in the dalyite structure. The low contents of Ti and Hf (up to 0.030 and 0.013 apfu, respectively), indicate that replacement of Zr with Ti and Hf is limited. These analyses suggest that the CCI dalyite corresponds to the more precise formula $(K_{1.79\text{-}1.87}Na_{0.12\text{-}0.19})(Zr_{0.90\text{-}0.96}\ Ti_{0.004\text{-}0.030}Hf_{0.010\text{-}0.013})(Si_{6.01\text{-}6.06}O_{15})$. Calculated alkalinity moduli (Khomyakov 1995) values range from 21.90 to 22.39. In addition to Na, Fe Ti and Hf, the data suggest that trace amounts of Al, Ba, Mg, and Mn may be present, though these are all very close to the detection limit. This is supported by their occurrence in trace amounts in various literature analyses (Table 1).

Solid state modelling

Calculated solution energies (E_{sol}) for a number of potential substitutions are presented in Table 6. In each instance, the lowest E_{sol} value is considered to highlight the most likely substitution. Model results for Ti indicate Ti↔Si substitution as the most energetically favourable (E_{sol} = - 0.98 eV), though Ti↔Zr substitution is also likely (E_{sol} = - 0.25 eV). Modelling of Hf is more conclusive, with Hf↔Zr substitution representing the most likely scenario (E_{sol} = - 0.31 eV). The incorporation of the R^{2+} cations Fe^{2+}, Mg^{2+} and Ba^{2+} was also modelled, but charge balancing necessitates the presence of site vacancies, in this case assumed to be a single O vacancy. Results indicate that, in the case of Fe^{2+} and Mg^{2+} the lowest energy scenario is replacement of K. Nevertheless, the calculated E_{sol} values of 8.86 eV and 9.61 eV, respectively, highlight the overall difficulty of their inclusion within the dalyite structure. Modelling of Ba yields a similar result, though the calculated E_{sol} value of 4.94 eV for Ba↔K substitution is noticeably lower than other R^{2+} cations.

Discussion

Variations in dalyite chemical composition

To facilitate a wider discussion of the compositional variability of dalyite, all available analyses are divided into two groups: 1) those found within peralkaline syenitic or granitic rocks and 2) those found within other lithologies, including lamproites, lamprophyres and charoitites. As such, the dalyite analyses from Terceira, São Miguel, Ascension, Straumsvola, Strange Lake and Gordon Butte are included in group 1, whereas analyses from Sunnfjord, Murun and Cancarix occupy group 2. All analyses were tested for quality using the following criteria: a) analysis total = 100 wt. % ± 1.5, b) total cations = < 9.05 apfu, c) cation total for the tetrahedral site = 6 apfu ± 0.05, d) cation total for the octahedral site = 1 apfu ± 0.05. Only those analyses which passed all four criteria were applied to the following discussion, reducing the size of dataset from 43 to 25 analyses.

The overall average calculated K_{alk} for the combined dataset is 21.94, with minimum and maximum values of 20.90 and 22.51, respectively. This shows

287 essentially no variation between groups 1 and 2, with average values of 21.98 and
288 21.91, respectively.

289 Figure 3a shows the available dalyite analyses in K–Na space. The data
290 typically lie within 0.05 apfu of the one-to-one line, indicating the role of one-to-one
291 K↔Na substitution within the polyhedral sites. Group 1 analyses are characterised
292 by a relative abundance of Na (0.12 to 0.19 apfu) and a corresponding paucity of K
293 (1.79 to 1.87 apfu), though two analyses from Straumsvola and Strange Lake
294 (analyses 3 & 4, Table 1) exhibit Na concentrations below the detection limit,
295 alongside a slight deficiency in K. This discrepancy in older dalyite analyses may
296 indicate Na loss during analysis, as suggested by Birkett et al. (1992). The dalyite
297 from Strange Lake may also have been subject to alteration, as it is described as
298 being frequently rimmed by elpidite or vlasovite.

299 In contrast to group 1, group 2 analyses are closer to the ideal dalyite
300 formula, with significantly lower concentrations of Na (< 0.015 to 0.03 apfu). The
301 relatively sodic nature of group 1 and potassic nature of group 2 dalyite correlates
302 with the relatively sodic nature of the group 1 rocks and the generally potassic
303 nature of group 2 rocks. For example, reported whole rock Na_2O/K_2O ratios of
304 group 1 typically lie between 1 and 1.5 (Harris and Rickard, 1987; Ridolfi et al.,
305 2003; this study). In contrast, group 2 whole rock Na_2O/K_2O is likely to be
306 significantly lower, given their often highly potassic nature, as is the case for the
307 Cancarix dalyite (Na_2O/K_2O = 0.1, Linthout et al., 1988; Salvioli-Mariani &
308 Venturelli, 1996). Harris & Rickard (1987) made a similar observation, noting that
309 the dalyite analyses from Sunnfjord (analyses 16 to 25, Table 1) exhibit lower Na
310 contents than dalyite from Ascension Island (analysis 2, Table 1), which they
311 attributed to the higher Na_2O/K_2O ratio of the latter. However, they also noted that
312 Straumsvola dalyite (analysis 3, Table 1) has essentially no Na, despite a highly
313 comparable Na_2O/K_2O ratio to that of group 1 samples (1.35).

314 Another potential control that must be considered is the crystallisation
315 mechanism of each example, which must also play a role in the composition of
316 dalyite. For example, the dalyite-bearing, ultrapotassic Sunnfjord dyke is reported
317 to be heavily hydrothermally-altered (Furnes et al., 1982), suggesting that any
318 dalyite present may be metasomatic in origin, or a magmatic composition that has

been altered by metasomatism. It can be seen in Table 1 that those analyses which may have been influenced by metasomatism (e.g. Sunnfjord, Murun) frequently exhibit Na contents below detection. However, although the Straumsvola analysis (itself an average of three analyses) contains no significant Na, the peralkaline granite host rock is described as being very fresh (Harris & Rickard, 1987), and so the reported Na-poor dalyite cannot be attributed entirely to the effects of crystallisation mechanism or alteration.

The degree of substitution within the octahedral sites is highlighted in Figure 3b. Ti and Hf are considered as the most suitable substitutes, though the R^{2+} cations Mg, Mn and Fe are also considered (where data is available), due to the similarity of their ionic radii with Zr. In Figure 3b, the data plot within 0.05 apfu of the one-to-one line, indicating one-to-one cation exchange. In the case of Fe, Mn and Mg, this would introduce a charge imbalance which can be mitigated by a single oxygen vacancy. Although solid-state modelling suggests that $R^{2+}\leftrightarrow K$ substitution should be energetically favourable, the calculated E_{sol} values are still too large (8.86 eV & 9.61 eV), and the difference in ionic radii too great, to fully justify the placement of R^{2+} cations in the polyhedral sites. The substitutions of Hf↔Zr and Ti↔Zr are both supported by solid-state modelling (E_{sol} = -0.31 eV & -0.25 eV, respectively, though in the latter case, the modelling also indicates the potential of Ti↔Si substitution (E_{sol} = -0.98 eV). However, there is no evidence within the dataset to support such a substitution.

Group 1 analyses remain close to the ideal dalyite formula, with 0.91 to 0.98 apfu Zr. Group 2 analyses exhibit a greater degree of substitution, generally clustering between 0.85 and 0.94 apfu Zr, with 0.05 to 0.12 apfu Ti. It is notable that one of the two analyses from the charoitites of the Murun Complex is enriched in the davanite component ($K_2TiSi_6O_{15}$), with 0.21 apfu Ti. This may relate to the unusual nature of their charoititic host rock, which is typically considered to be metasomatic rather than magmatic in origin (e.g. Reguir, 2001 and references therein). This alternative origin may explain the apparent geochemical deviation from the rest of the dataset.

The dataset indicates the presence of small amounts of Ba within Group 2 dalyite. On the basis of solid-state modelling and ionic radii, it is suggested that the

most likely mechanism for its inclusion within the dalyite structure is Ba↔K. The resulting charge imbalance could be mitigated by a single vacancy in the polyhedral site, in which case the Ba content may be used as a proxy for the polyhedral vacancies in each analysis (up to 0.02 apfu). This may, in part, account for analyses in which the structural total is less than the ideal 9 apfu. Alternatively, structural deficits may result from the presence of Li. Significant concentrations of Li have been reported in peralkaline rocks and Li-enrichment can occur via metasomatic processes (e.g. Borley, 1963; Hawthorne et al., 1996; Brenan et al., 1998; Hawthorne et al., 2001). Although the mechanisms of Li-substitution in dalyite are unclear, its inclusion may contribute to the frequently low structural totals observed within the dataset.

The key geochemical parameters required to stabilise dalyite are high μK_2O and high $aSiO_2$ (Marks et al., 2011). For example, an insufficiently high silica activity will lead to the crystallisation of wadeite ($K_2ZrSi_3O_9$) in place of dalyite (Marks et al., 2011). Dalyite is therefore limited to silica-saturated to –oversaturated lithologies, although its occurrence in a nepheline-bearing pegmatite from Langesundfjord, Norway (Andersen et al., 2010) appears to contradict this. The additional requirement of high μK_2O is likely due to high K_2O contents in the melts, achieved either by slowly increasing K_2O via fractional crystallisation and/or crustal assimilation of potassic rocks in the group 1 samples, or by producing melts with initially high K_2O values via the more unusual processes suggested to produce ultrapotassic rocks, such as partial melting of metasomatised mantle lithologies, (e.g. Mitchell & Bergman, 1991).

The geochemical variations observed between the groups of this study are likely to represent major element variations in the melts themselves. For example, the group 2 dalyites generally show elevated Ti and Fe contents relative to the group 1 dalyites, which may relate to the relatively Ti- and Fe-rich whole rock compositions of lamproites and lamprophyres, particularly when compared to the low Ti contents of group 1 whole rock analyses (< 0.7 wt. %). Additionally, group 2 analyses exhibit significantly lower degrees of Na substituting for K, which might be expected given the K_2O-rich nature of their whole rock analyses.

383 *Dalyite crystallisation on Terceira*

384 Dalyite is generally considered to be a late-stage, magmatic mineral phase (e.g.
385 Harris & Rickard, 1987; Ridolfi et al., 2003) that may be altered, either during later
386 magmatic or sub-solidus stages, to minerals such as elpidite, $Na_2ZrSi_6O_{15}\cdot 3(H_2O)$
387 (Cann, 1967), catapleiite, $Na_2Zr(Si_3O_9)\cdot 2H_2O$ (Birkett et al., 1992; Chakhmouradian
388 & Mitchell, 2002) and intergrown quartz and zircon (Cann, 1967). Key features of
389 the Terceira dalyite, notably the dominantly anhedral crystal forms, its restricted
390 occurrence in interstitial pore spaces and its lack of inclusion within other mineral
391 phases, all point towards late-stage, post-cumulus, magmatic crystallisation,
392 though extension of the crystallisation interval into the sub-solidus deuteric stage
393 cannot be ruled out. Evidence for the alteration of primary dalyite compositions is
394 lacking. Its textural association and occasional intergrowth with quartz suggests
395 that the crystallisation of these two phases was largely contemporaneous. This
396 conclusion is in agreement with that of Ridolfi et al. (2003), who studied similar
397 parageneses in syenite nodules erupted by Agua de Pau volcano, São Miguel,
398 Azores.

399 The dalyite analyses from Terceira display two clusters in Na-K space (Fig.
400 3a), with one cluster of more sodic compositions (0.17 to 0.19 Na apfu), and
401 another cluster of more potassic compositions (0.12 to 0.13 Na apfu). The
402 difference between these clusters cannot be entirely accounted for by the
403 calculated two-sigma errors of ±0.015 apfu, and is considered to represent
404 bimodality in the dataset. Both clusters lie within 0.05 apfu of the one-to-one line
405 and, as such, the trend of the data likely highlights the role of varying degrees of
406 one-to-one Na↔K substitution within the Terceira samples. The presence of two
407 subgroups may imply that two separate populations of dalyite are present, either
408 derived from multiple processes that each led to the crystallisation of
409 compositionally distinct dalyite, or a single process that is capable of producing a
410 heterogeneous dalyite population. No visible correlation exists between dalyite
411 composition and textural features such as crystal form or size, or the degree to
412 which they infill pores. Instead, the two clusters of dalyite analyses can be related
413 to the two separate samples in which dalyite was analysed (TER-30-1 and TER 30-

7), with the most sodic dalyite analyses being from TER 30-1. The compositional variations may therefore reflect random sampling of a syenitic mush in which geochemical heterogeneity is sufficiently large in scale that it yields 'inter-nodule' variations in dalyite composition, whilst 'intra-nodule' variations are more limited. Such heterogeneity may be primary (i.e. derived from original compositional variations in the melt, perhaps originating from multiple magma batches that contributed to a single crystal mush body), or secondary, originating from the variable degree of fluid-feldspar reaction (albitization; e.g. Lee & Parsons, 1997) in the crystal mush during deuteric alteration. The late stage albitization of the rock would lead to a bulk rock increase in Na and an enrichment of K in the albitizing fluids. The prevalence of coarse patchy perthitic feldspars in the Terceira syenites provides evidence for the prominent role of albitization in their late stage evolution. Evidence for primary bulk compositions being the underlying control upon dalyite composition exists in the bimodality of the dataset, with the most sodic dalyites found in the most sodic whole rock analysis.

However, a single analysis from sample TER 30-7 falls within the cluster of TER 30-1 analyses (Fig. 2a, Table 5), indicating that a simple relationship between dalyite chemistry and bulk rock composition cannot entirely account for the observed variation. As such, alternative processes that might influence the degree of Na↔K substitution are explored. One example that is considered here is the role of variable pore size in the compositional evolution of interstitial melts. Because heterogeneous nucleation is energetically favourable compared to homogenous nucleation, the dominant process that drives the compositional evolution of a melt within a pore under closed system conditions is the crystallisation of surrounding cumulus phases, as components that are incompatible in the pore wall minerals become enriched in the residual melt. In the Terceira syenite nodules, alkali-feldspar is the most abundant phase, and surrounds the majority of pore spaces, suggesting that the post-cumulus, heterogeneous nucleation of feldspar onto pore walls will exert the strongest influence upon interstitial melt compositions. Due to its albite-rich composition (~ Ab_{64}, average Na/K = 1.67) (A. J. Jeffery, unpublished data), this effect is likely to promote the development of depressed Na/K ratios in the liquid as evolution continues. Petrographic evidence for this process exists in

446 the form of optically distinguishable rims on many of the pore-wall feldspars (e.g.
447 Fig. 2c). During the sub-solidus deuteric stage, albitization also contributes to the
448 depression of liquid Na/K ratios via the replacement of alkali feldspar with near end
449 member albite. Thus, it is suggested that during the late stage magmatic and sub-
450 solidus deuteric evolution of the syenite, the majority of liquid-filled pores were
451 evolving towards more potassic compositions.

452 It is proposed that the observed variation in Terceira dalyite composition
453 could be related to the timing of crystallisation relative to the evolution of the
454 interstitial melt. The thermodynamics of crystallisation in pore spaces has been
455 shown to be fundamentally different compared to a free fluid (Bigg, 1953; Melia &
456 Moffitt, 1964; Putnis et al., 1995; Scherer, 1999). In particular, a fluid confined to a
457 pore space can achieve greater degrees of supersaturation prior to the onset of
458 crystallisation compared with an unconfined fluid, thus introducing a nucleation
459 delay that is more substantial in smaller pores (e.g. Putnis & Mauthe, 2001;
460 Holness et al., 2007; Holness & Sawyer, 2008). As such, the dalyite crystals that
461 grew in smaller pores would have nucleated later than those in larger pores, and
462 would record more evolved compositions. Holness & Sawyer (2008) also cited the
463 prevalence of single-grain pseudomorphs in small pores and poly-mineralic
464 aggregate pseudomorphs in larger pores as petrographic evidence for the relative
465 ease of nucleation in larger pores. This feature can also be observed in the CCI
466 syenite, where larger pores are frequently filled with aggregates of late-crystallising
467 phases such as quartz, clinopyroxene, dalyite, and eudialyte (Fig. 2f), whilst small
468 pores generally contain only a single crystal of one of these phases (Fig. 2d).

469 Considering the previously described evolutionary trend of relative K-
470 enrichment during both late stage magmatic and sub-solidus stages, dalyite in
471 smaller pores should therefore have more potassic compositions. To test this
472 hypothesis, dalyite-bearing pore spaces were digitised and measured using
473 ImageJ to determine the two-dimensional area. This was then plotted against the
474 Na content of the dalyite crystal within them (Fig. 4), yielding a positive correlation
475 that suggests that the size of a pore exerts, at least to some extent, a control over
476 the composition of the dalyite crystallising within it.

A single data point in Fig. 4 appears to deviate from the broadly linear trend observed in the rest of the data (pore area = 1.07 mm^2, Na content = 0.18). Unlike other reported dalyites, this dalyite crystal is found in a pore that is bounded by a large clinopyroxene crystal, in addition to alkali-feldspar. It is therefore suggested that this deviation in pore size vs. Na content space may highlight the influence of other minerals in the evolution of interstitial melts. Given the relatively high Na contents and negligible K contents of the Terceira clinopyroxene (Na/K = 6 to 2584) (A. J. Jeffery, unpublished data), the pore wall crystallisation of clinopyroxene would greatly accelerate the described evolutionary trend of K-enrichment in interstitial melt, leading to dalyite compositions that appear unusually K-rich when compared with the suggested feldspar-controlled trend (Fig. 4). The pore wall crystallisation of amphibole would also produce this effect but to a lesser degree (Na/K = 5.7 to 8.9) (A. J. Jeffery, unpublished data).

In summary, it is suggested that the dalyite from Terceira is predominantly late-stage magmatic in origin, and the observed compositional variability is influenced by the K-enrichment trend of late stage interstitial melt resulting from pore wall crystallisation of sodic alkali feldspar. Any continued crystallisation during a sub-solidus deuteric stage is considered to have been subject to a similar K-enrichment trend, driven by albitization of alkali feldspar. Variation in Na content is likely to have been controlled, at least in part, by the larger nucleation delay that is introduced in smaller pores compared to larger ones.

Conclusions

A new occurrence of the rare potassium zirconium dalyite is reported from Terceira, Azores. The detailed study of new quantitative analyses of dalyite from Terceira, alongside solid state modelling and previously published analyses, allows the following conclusions to be made regarding the compositional variability of dalyite:

(1) Substitution of Na for K in dalyite is generally more significant in peralkaline granites and syenites than in highly potassic rock types.

(2) The incorporation of small amounts of Ba occurs in potassic rocks and is most likely achieved via Ba↔K substitution..

(3) The incorporation of Fe into dalyite is minimal in peralkaline granites and syenites, but becomes more significant in highly potassic lithologies. Mineral chemical data and solid state modelling suggest that this is most easily achieved via Fe^{2+}↔Zr substitution, though high E_{sol} values and charge balancing requirements must hinder this relationship.

(4) The degree of substitution of Ti for Zr is greater in highly potassic igneous rocks than in peralkaline granites and syenites, and may be linked to elevated Ti-contents of the melts.

(5) The dalyite from Terceira shows variation in the degree of Na↔K substitution that does not relate obviously to texture, and cannot be entirely attributed to 'inter-nodule' diversity. This feature is linked to relative K-enrichment induced by the effects of pore wall crystallisation (during a late stage magmatic phase) and albitization (during a sub-solidus deuteric phase), coupled with the variation in nucleation delay that is introduced by variable pore sizes.

Acknowledgements

We gratefully acknowledge S. Self, A. Pimentel, J. Pacheco and the Centro de Vulcanologia e Avaliação de Riscos Geológicos (CVARG) for their invaluable assistance and logistical support during fieldwork. We are grateful to P. Williams and R. Mitchell for editorial handling, and F. Ridolfi and G. Gatta for their detailed and constructive comments, which greatly improved the manuscript. E. Reguir is thanked for kindly providing a copy of Table 48 from Konev et al. (1996).

References

Akhtar, M. J., Waseem, S. (2001) Atomistic simulation studies of zircon. Chemical Physics**,** 274: 109-120

Andersen, T., Erambert, M., Larsen, A. O., Selbekk, R. S. (2010) Petrology of nepheline syenite pegmatites in the Oslo Rift, Norway: zirconium silicate mineral assemblages as indicators of alkalinity and volatile fugacity in mildly agpaitic magma. Journal of Petrology, 51: 2303-2325

Bigg, E. K. (1953) The supercooling of water. Proceedings of the Physical Society (London), 66B: 688-694

Birkett, T. C., Miller, R. R., Roberts, A. C., Mariano, A. N. (1992) Zirconium-bearing minerals of the Strange Lake Intrusive Complex, Quebec-Labrador. Canadian Mineralogist, 30: 191-205

Borley, G. D. (1963) Amphiboles from the Younger Granites of Nigeria. I. Chemical classification. Mineralogical Magazine, 33: 358-376

Brenan, J. M., Neroda, E., Lundstrom, C. C., Shaw, H. F., Ryerson, F. J., Phinney, D. L. (1998) Behaviour of boron, beryllium, and lithium during melting and crystallization: constraints from mineral-melt partitioning experiments. Geochimica et Cosmochimica Acta, 62: 2129-2141

Brod, J. A. (1999) Petrology and geochemistry of the tapira alkaline complex, minas gerais state, Brazil. [Ph.D. thesis]. Durham University, U.K., 486 pp.

Cann, J. R. (1967) A second occurrence of dalyite and the petrology of some ejected syenite blocks from São Miguel, Azores. Mineralogical Magazine, 36: 227-232

565 Chakhmouradian, A. R., Mitchell, R. H. (2002) The mineralogy of Ba- and Zr-rich
566 alkaline pegmatites from Gordon Butte, Crazy Mountains (Montana, USA):
567 comparisons between potassic and sodic agpaitic pegmatites. Contributions to
568 Mineralogy and Petrology, 143: 93-114
569
570 Dolivo-Dobrovol'skiy, D. V., Yevdokimov, M. D. (1991) Zirconium mineralisation of
571 the alkali metasomatites of the Murun Complex. International Geology Review, 33:
572 490-496
573
574 Fleet, S. G. (1965) The crystal structure of dalyite. Zeitschrift für Kristallographie,
575 121: 349-368
576
577 Furnes, H., Mitchell, J. G., Robins, B., Ryan, P., Skjerlie, F. J. (1982) Petrography
578 and geochemistry of peralkaline, ultrapotassic syenite dykes of Middle Permian
579 age, Sunnfjord, West Norway. Norsk Geologisk Tidsskrift, 62: 147-159
580
581 Gale, J. D. (1997) GULP: A computer program for the symmetry-adapted
582 simulation of solids. Journal of the Chemical Society, Faraday Transactions, 93:
583 629-637
584
585 Gente, P., Dyment, J., Maia, M., Goslin, J. (2003) Interaction between the Mid-
586 Atlantic Ridge and the Azores hot spot during the last 85 Myr: emplacement and
587 rifting of the hotspot derived plateaus. Geochemistry, Geophysics, Geosystems, 4:
588 8514, doi: 10.1029/2003GC000527
589
590 Gertisser, R., Self, S., Gaspar, J. L., Kelley, S. P., Pimentel, A., Eikenberg, J.,
591 Barry, T. L., Pacheco, J. M., Queiroz, G., Vespa, M. (2010) Ignimbrite stratigraphy
592 and chronology on Terceira Island, Azores. The Geological Society of America,
593 Special Paper 464: 133-154
594

595 Harris, C., Cressey, G., Bell, J. D., Atkins, F. B., Beswetherick, S. (1982) An
596 occurrence of rare-earth-rich eudialyte from Ascension Island, South Atlantic.
597 Mineralogical Magazine, 46: 421-425
598
599 Harris, C., Rickard, R. S. (1987) Rare-earth-rich eudialyte and dalyite from a
600 peralkaline granite dyke at Straumsvola, Dronning Maud Land, Antarctica. The
601 Canadian Mineralogist, 25: 755-762
602
603 Hawthorne, F. C., Oberti, R., Ottolini, L., Foord, E. E. (1996) Lithium-bearing fluor-
604 arfvedsonite from Hurricane Mountain, New Hampshire: a crystal-chemical study.
605 The Canadian Mineralogist, 34: 1015-1019
606
607 Hawthorne, F. C., Oberti, R., Cannillo, E., Ottolini, L., Roelofsen, J. N., Martin, R. F.
608 (2001) Li-bearing arfvedsonitic amphiboles from the Strange Lake peralkaline
609 granite, Quebec. The Canadian Mineralogist, 39: 1161-1170
610
611 Holness, M. B., Anderson, A. T., Martin, V. M., Maclennan, J., Passmore, E.,
612 Schwindinger, K. (2007) Textures in partially solidified crystalline nodules: a
613 window into the pore structure of slowly cooled mafic intrusions. Journal of
614 Petrology, 48: 1243-1264
615
616 Holness, M. B., Sawyer, E. W. (2008) On the pseudomorphing of melt-filled pores
617 during crystallization of migmatites. Journal of Petrology, 49: 1343-1363
618
619 Khomyakov, A. P. (1995) Mineralogy of hyperagpaitic alkaline rocks. Oxford
620 Science Publications, Oxford, UK. 222 pp.
621
622 Konev, A. A., Vorob'ev, E. I., Lasebnik, K. A. (1996) The mineralogy of the Murun
623 alkaline massif. Siberian Branch of the Russian Academy, Scientific Press,
624 Novosibirsk, (in Russ.)
625

626 Krause, D. C., Watkins, N. D. (1970) North Atlantic crustal genesis in the vicinity of
627 the Azores. Geophysical Journal of the Royal Astronomical Society, 19: 261-283
628
629 Kröger, F. A., Vink, H. J. (1956) Relations between the concentrations of
630 imperfections in crystalline solids. Solid State Physics, 3, 307-435
631
632 Lazebnik, K. A., Makhotko, V. F. (1982) Dalyite, the first finding in the USSR.
633 Zapiski Vsesoyuznogo Mineralogicheskogo Obschestva, 111: 587-593
634
635 Lee, M. R., Parsons, I. (1997) Dislocation formation and albitization in alkali
636 feldspars from the Shap granite. American Mineralogist, 82: 557-570
637
638 Linthout, K., Nobel, F. A., Lustenhouwer, W. J. (1988) First occurrence of dalyite in
639 extrusive rock. Mineralogical Magazine, 52: 705-708
640
641 Mariano, A. N., Francis, C. A. (1989) Dalyite from fenites in carbonatite complexes
642 of the Minas Gerais – Goias belt, Brazil. Geological Society of America Abstract
643 Programs, 21: A46
644
645 Mariano, A. N., Marchetto, M. (1991) Serra Negra and Salitre – carbonatite alkaline
646 igneous complex. In: Leonardos, O. H., Meyer, H. O. A., Gaspar, J. C. (Eds) 5th
647 International Kimberlite Conference (Field Guide Book). Araxá, Brazil, CPRM,
648 Special publication, 3/91: 75-79
649
650 Marks, M. A. W., Hettmann, K., Schilling, J., Frost, B. R., Markl, G. (2011) The
651 mineralogical diversity of alkaline igneous rocks: critical factors for the transition
652 from miaskitic to agpaitic phase assemblages. Journal of Petrology, 52: 439-455
653
654 Melia, T. P., Moffitt, W. P. (1964) Crystallisation from aqueous solution. Journal of
655 Colloid Science, 19: 433-447
656

Mitchell, R. H., Bergman, S. C. (1991) Petrology of lamproites. New York/London: Plenum Press. 447 pp.

Mujaji, M., Burrows, J., Jackson, R. A. (2014) Optical spectroscopy of the Nd^{3+} and Nd^{3+} - Gd^{3+}/Yb^{3+} centres in BaF_2 single crystals and calculations on lanthanide-doped BaF_2. Journal of Luminescence, 151: 106-110

Putnis, A., Mauthe, G. (2001) The effect of pore size on cementation in porous rocks. Geofluids, 1: 37-41

Putnis, A., Prieto, M., Fernandez-Diaz, L. (1995) Supersaturation and crystallisation in porous media. Geological Magazine, 132: 1-13

Raade, G., Mladeck, M. H. (1983) Janhaugite, $Na_3Mn_3Ti_2Si_4O_{15}(OH,F,O)_3$, a new mineral from Norway. American Mineralogist, 68: 1216-1219

Reguir, E. (2001) Aspects of the mineralogy of the Murun alkaline complex, Yakutia, Russia. [M.Sc thesis]. Lakehead University, Canada, 193 pp.

Ridolfi, F., Renzulli, A., Santi, P., Upton, B. G. J. (2003) Evolutionary stages of crystallization of weakly peralkaline syenites: evidence from ejecta in the plinian deposits of Agua de Pau volcano (Sao Miguel, Azores Islands). Mineralogical Magazine, 67: 749-767

Robins, B., Furnes, H., Ryan, P. (1983) A new occurrence of dalyite. Mineralogical Magazine, 47: 93-94

Saleh, G. M. (2006) Geologic relationships and mineralisation of peralkaline/alkaline granite-syenite of the Zargat Na'am ring complex, Southeastern Desert, Egypt. Chinese Journal of Geochemistry, 25: 97-111

688 Salvi, S., Williams-Jones, A. E. (1995) Zirconosilicate phase relations in the
689 Strange Lake (Lac Brisson) pluton, Quebec-Labrador, Canada. American
690 Mineralogist, 80: 1031-1040
691
692 Salvioli-Mariani, E., Venturelli, G. (1996) Temperature of crystallisation and
693 evolution of the Jumilla and Cancarix lamproites (SE Spain) as suggested by melt
694 and solid inclusions in minerals. European Journal of Mineralogy, 8: 1027-1039
695
696 Scherer, G. W. (1999) Crystallization in pores. Cement and Concrete Research,
697 29:1347-1358
698
699 Schmitt, A. K., Emmermann, R., Trumbull, R. B., Bühn, B., Henjes-Kunst, F. (2000)
700 Petrogenesis and $^{40}Ar/^{39}Ar$ geochronology of the Brandberg Complex, Namibia:
701 evidence for a major mantle contribution in metaluminous and peralkaline granites.
702 Journal of Petrology, 41: 1207-1239
703
704 Self, S. (1974) Recent volcanism on Terceira, Azores. [Ph.D. thesis]. Imperial
705 College, U.K., 236 pp.
706
707 Self, S. (1976) The recent volcanology of Terceira, Azores. Journal of the
708 Geological Society, 132: 645-666
709
710 Stepnova, Y. A., Zalishchak, B. L., Pakhomova, V. A. (2013) Rare-earth
711 mineralisation of alkali magma of the Russian Far East: on the example of the
712 Shibanovsky massif. Геология, Вестник, 3: 44-51 (in Russ.)
713
714 Van Tassel, R. (1952) Dalyite, a new potassium zirconium silicate, from Ascension
715 Island, Atlantic. Mineralogical Magazine, 29: 850-857
716
717 Venturelli, G., Capedri, S.,Di Battistini, G., Crawford, A., Kogarko, L. N., Celestini,
718 S. (1984) The ultrapotassic rocks from southeastern Spain. Lithos, 17: 37-54
719

720 Widom, E., Gill, J. B., Schmincke, H. -U. (1993) Syenite nodules as a long-term
721 record of magmatic activity in Agua de Pau volcano, São Miguel, Azores. Journal
722 of Petrology, 34: 929-953

Figure captions

Figure 1 Reported occurrences of dalyite worldwide. **1)** Ascension Island, South Atlantic Ocean (Van Tassel, 1952) **2)** Agua de Pau volcano, São Miguel, Azores (Cann, 1967) **3)** the Murun Complex, Siberia, Russia (Lazebnik & Makhotko, 1982; Dolivo-Dobrovol'skiy & Yevdokimov, 1991; Konev et al., 1996; Reguir, 2001) **4)** Gjerdingen, Norway (Raade & Mladeck, 1983) **5)** Sunnfjord, Norway (Furnes et al., 1982; Robins et al., 1983) **6)** the Straumsvola Complex, Dronning Maud Land, Antarctica (Harris & Rickard, 1987) **7)** Cancarix, South Eastern Spain (Venturelli et al., 1984; Linthout et al., 1988) **8)** the Serra Negra and Salitre Complex, Brazil (Mariano & Francis, 1989; Mariano & Marchetto, 1991) **9)** the Strange Lake Complex, Canada (Birkett et al., 1992; Salvi & Williams-Jones, 1995) **10)** the Brandberg Complex, Namibia (Schmitt et al., 2000) **11)** Gordon Butte, Montana, USA (Chakhmouradian & Mitchell, 2002) **12)** the Zargat Na'am ring complex, Egypt (Saleh, 2006) **13)** Langesundfjord, Norway (Andersen, et al., 2010) **14)** the Shibanovsky Massif, Russia (Stepnova et al., 2013) **15)** Terceira Island, Azores (this study)

Figure 2 a) Example of a fine to medium grained, alkali-feldspar dominated nodule. The feldspars appear altered and are often perthitic. A large, optically-continuous quartz crystal is highlighted with a white box in the lower right corner of the image. **b)** A medium to coarse grained nodule with larger crystal sizes and fresher, less-altered feldspars **c)** A large dalyite crystal which partially infills an interstitial void between larger alkali-feldspar crystals. Also visible are small amphibole crystals and stellate clinopyroxene **d)** An anhedral dalyite crystal which partially fills an interstitial void between large alkali-feldspars and a large amphibole crystal **e)** An anhedral dalyite crystal forming an incomplete rim around the edges of an interstitial cavity. A small clinopyroxene crystal appears to have been included within the dalyite. A resorbed, optically distinctive feldspar core is visible within the large feldspar to the lower right of the image **f)** An element map highlighting a large, anhedral dalyite crystal filling an interstitial space, together with intergrown quartz and small amounts of clinopyroxene. Colours used: Red = Fe, Purple = Zr, Blue = Si, Green = Al. Abbreviations used: Qtz = quartz, Fsp = alkali-feldspar, Amp = amphibole, Cpx = Clinopyroxene, Dal = dalyite

Figure 3 Geochemical variation diagrams highlighting the variable degree of substitution within the dataset. The ideal composition of dalyite is highlighted with a black star symbol. The maximum error is applicable to the new data for Terceira (TER 30-1 and TER 30-7) only and is calculated as described in the text. Group 1 dalyite is denoted by diamonds, group 2 by triangles. Only analyses that passed all of the filtering criteria described in the text are shown **a)** Bivariate plot showing the degree of K↔Na substitution in the dataset. **b)** Bivariate plot showing the degree of substitution in the octahedral site. Data for Hf, Mg and Fe is presented where analyses permit

Figure 4 Bivariate plot of measured pore area against the Na content of dalyite within the pore

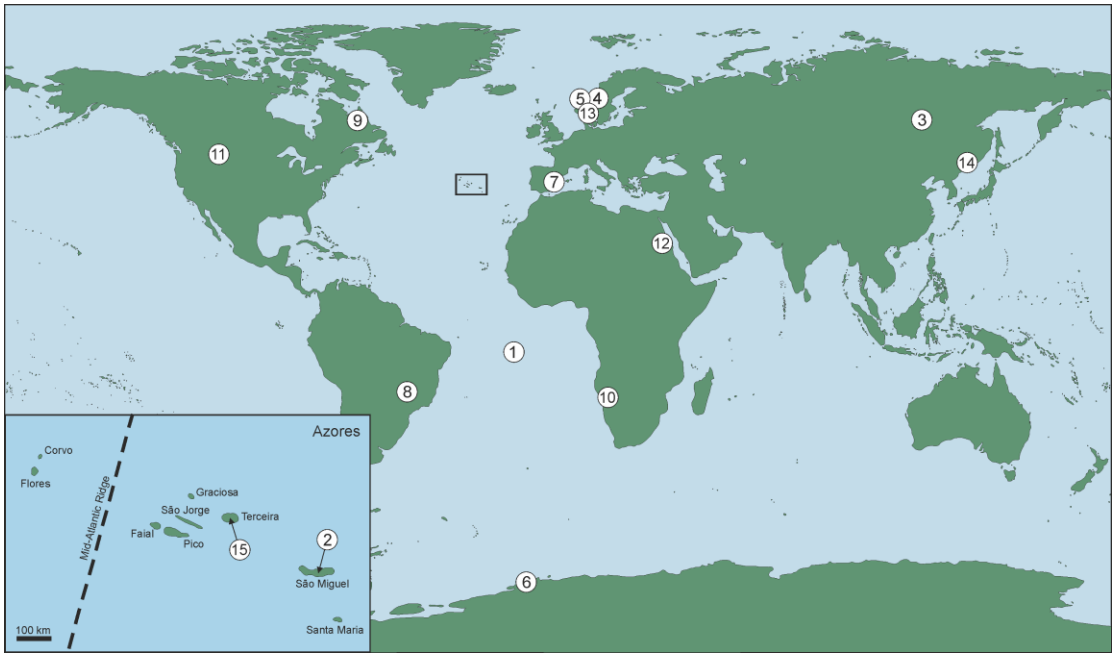
Azores
Corvo
Flores
Graciosa
São Jorge
Terceira
Faial
Pico
São Miguel
Santa Maria
Mid-Atlantic Ridge
100 km
1
2
3
4
5
6
7
8
9
10
11
12
13
14
15

Figure 1

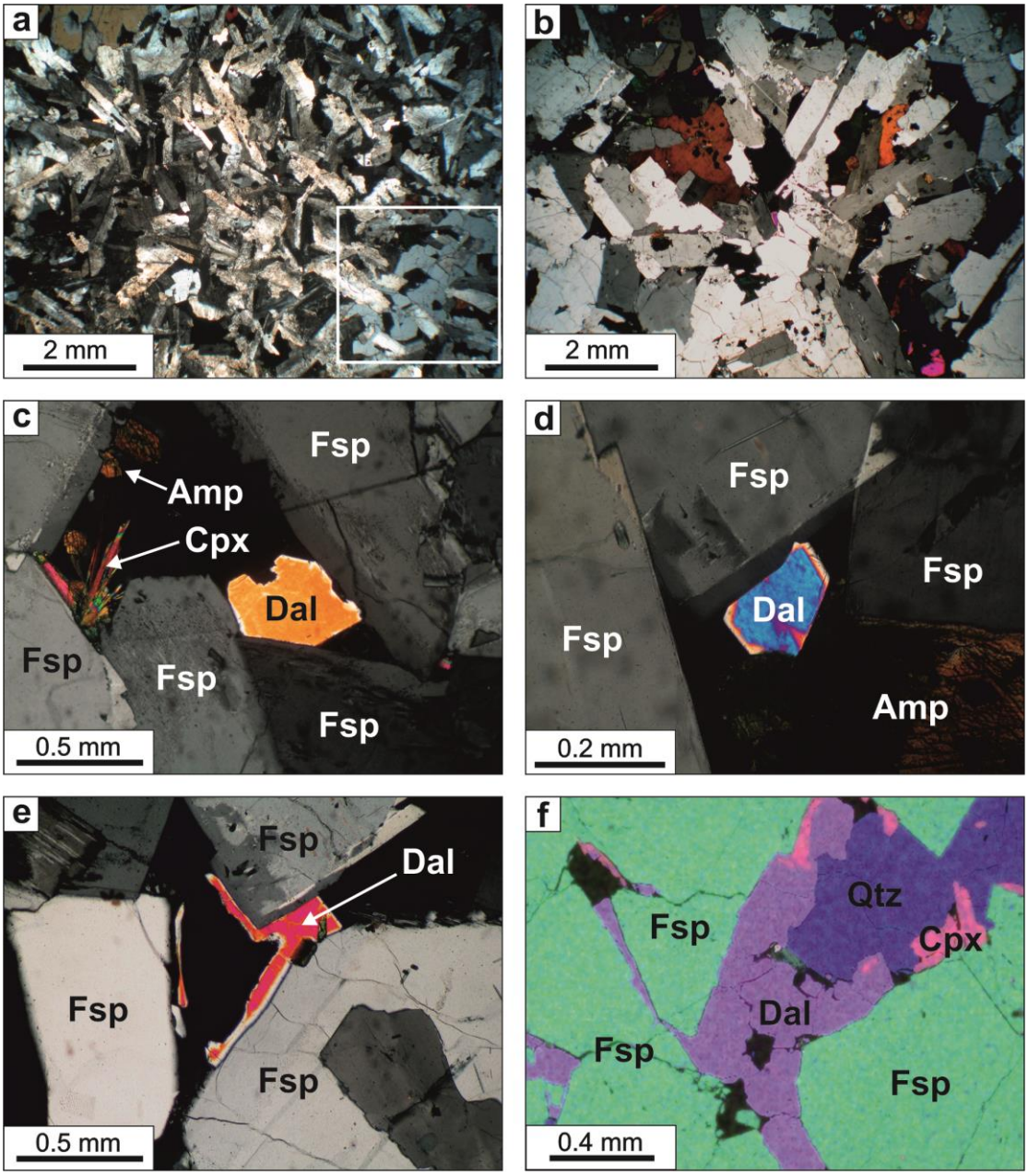
a
2 mm
b
2 mm
c
Fsp
Amp
Cpx
Dal
Fsp
Fsp
Fsp
0.5 mm
d
Fsp
Fsp
Dal
Fsp
Amp
0.2 mm
e
Fsp
Dal
Fsp
Fsp
0.5 mm
f
Qtz
Fsp
Cpx
Dal
Fsp
Fsp
0.4 mm

Figure 2

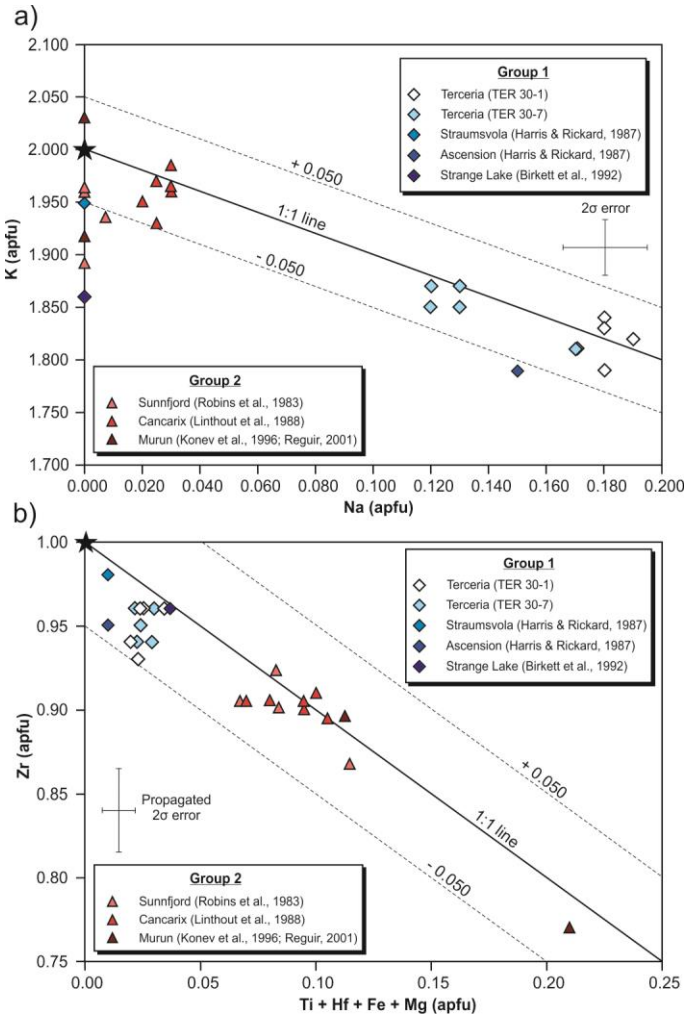
a)
K (apfu)
Na (apfu)
Group 1
Terceria (TER 30-1)
Terceria (TER 30-7)
Straumsvola (Harris & Rickard, 1987)
Ascension (Harris & Rickard, 1987)
Strange Lake (Birkett et al., 1992)
Group 2
Sunnfjord (Robins et al., 1983)
Cancarix (Linthout et al., 1988)
Murun (Konev et al., 1996; Reguir, 2001)
+ 0.050
1:1 line
- 0.050
2σ error
b)
Zr (apfu)
Ti + Hf + Fe + Mg (apfu)
Propagated
2σ error

Figure 3

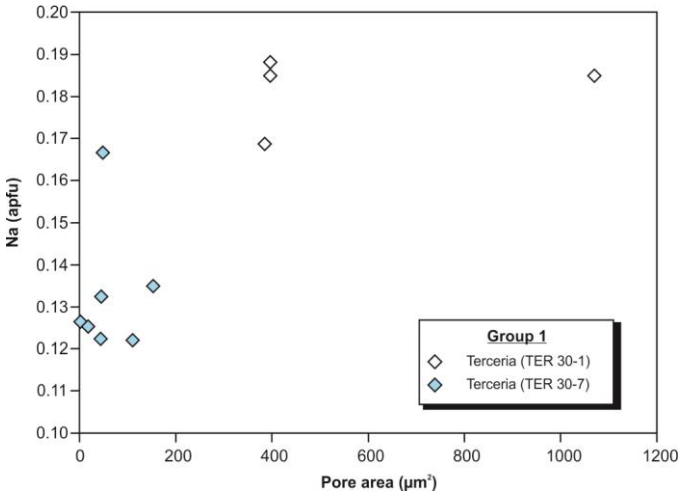
0.20
0.19
0.18
0.17
0.16
0.15
0.14
0.13
0.12
0.11
0.10
Na (apfu)
0
200
400
600
800
1000
1200
Pore area (µm²)
Group 1
Terceria (TER 30-1)
Terceria (TER 30-7)

Figure 4

Table 1 Literature electron microprobe analyses of dalyite

Location	**Ascension**	**Ascension**	**Straumsvola**	**Strange Lake**	**Gordon Butte**	**Agua de Pau**	**Agua de Pau**	**Agua de Pau**	**Agua de Pau**
Group	1	1	1	1	1	1	1	1	1
Host rock	Granite ejecta	Granite ejecta	Granite dyke	Granite	Alkaline pegmatite	Syenitic ejecta	Syenitic ejecta	Syenitic ejecta	Syenitic ejecta
Suggested origin	Magmatic	Magmatic	Magmatic	Magmatic	Magmatic	Magmatic	Magmatic	Magmatic	Magmatic
No.	1†	2*	3	4	5	6	7	8	9
SiO_2	61.85	63.25	62.07	62.55	60.35	62.23	61.35	61.35	61.36
TiO_2	-	0.12	0.13	0.08	1.78	0.08	0.11	0.14	0.15
Al_2O_3	-	-	-	*bdl*	*bdl*	-	-	-	-
FeO	0.33	0.03	*bdl*	0.06	0.18	-	-	-	-
MnO	-	*bdl*	*bdl*	-	*bdl*	-	-	-	-
MgO	-	-	-	-	*bdl*	-	-	-	-
CaO	-	*bdl*	*bdl*	*bdl*	*bdl*	-	-	-	-
Na_2O	1.75	0.79	*bdl*	*bdl*	0.02	0.69	0.37	0.44	0.49
K_2O	14.60	14.63	15.71	15.08	15.34	13.80	14.56	14.60	14.72
ZrO_2	21.70	20.43	20.63	20.38	18.21	23.72	23.57	23.27	23.49
HfO_2	-	-	-	0.81	-	-	-	-	-
BaO	-	-	-	-	*bdl*	-	-	-	-
P_2O_5	-	-	-	-	-	-	-	-	-
La_2O_3	-	*bdl*	*bdl*	0.04	-	-	-	-	-
Ce_2O_3	-	*bdl*	*bdl*	0.06	*bdl*	-	-	-	-
Nb_2O_5	-	*bdl*	*bdl*	-	1.65	-	-	-	-
Total	**100.23**	**99.25**	**98.54**	**98.96**	**97.53**	**100.52**	**99.96**	**99.80**	**100.21**
Si	5.94	6.05	6.03	6.04	5.92	5.94	5.92	5.92	5.91
Ti	-	0.01	0.01	0.01	0.13	0.01	0.01	0.01	0.01
Al	-	-	-	*bdl*	*bdl*	-	-	-	-
Fe	0.03	0.00	*bdl*	0.01	0.02	-	-	-	-
Mn	-	*bdl*	*bdl*	-	*bdl*	-	-	-	-
Mg	-	-	-	-	*bdl*	-	-	-	-
Ca	-	*bdl*	*bdl*	*bdl*	*bdl*	-	-	-	-
Na	0.33	0.15	*bdl*	*bdl*	0.00	0.13	0.07	0.08	0.09
K	1.79	1.79	1.95	1.86	1.92	1.68	1.79	1.80	1.81
Zr	1.02	0.95	0.98	0.96	0.87	1.10	1.11	1.10	1.10
Hf	-	-	-	0.02	-	-	-	-	-
Ba	-	-	-	-	*bdl*	-	-	-	-
P	-	-	-	-	-	-	-	-	-
La	-	*bdl*	*bdl*	0.00	-	-	-	-	-
Ce	-	*bdl*	*bdl*	0.00	*bdl*	-	-	-	-
Nb	-	*bdl*	*bdl*	-	0.07	-	-	-	-
Sum	**9.11**	**8.95**	**8.97**	**8.90**	**8.93**	**8.86**	**8.90**	**8.91**	**8.92**
K_{alk}	23.27	21.68	21.74	20.90	21.50	20.43	20.90	21.10	21.30

Analysis 1-2 from Ascension Island, (van Tassel, 1952; Harris & Rickard, 1987), analysis 3 from Straumsvola, Antarctica (Harris & Rickard, 1987), analysis 4 from the Strange Lake complex, Canada (Birkett et al., 1992), analysis 5 from Gordon Butte, USA (Chakhmouradian & Mitchell, 2002), analyses 6-9 from Agua de Pau, São Miguel Island (Ridolfi et al., 2003), analyses 10-15 from the Murun complex, Russia (Lazebnik & Makhotko, 1982; Konev et al., 1996; Reguir, 2001), analyses 16-25 from Sunnfjord, Norway (Robins et al., 1983), , analyses 26-31 from Cancarix, Spain (Linthout et al., 1988). Abbreviations and symbols used: (-) = not analysed; † Analysis includes 0.64 wt. % H_2O; * Average of three analyses; bdl = below detection limit. K_{alk} calculated after Khomyakov, 1995. All structural formulae recalculated from reported weight percent oxide values

Table 1 continued

Location	**Murun**	**Murun**	**Murun**	**Murun**	**Murun**	**Murun**	**Sunnfjord**	**Sunnfjord**	**Sunnfjord**	**Sunnfjord**	**Sunnfjord**
Group	2	2	2	2	2	2	2	2	2	2	2
Host rock			Charoitite	Charoitite	Charoitite	Charoitite	Syenite dyke	Syenite dyke	Syenite dyke	Syenite dyke	Syenite dyke
Suggested origin	Magmatic or Metasomatic	Magmatic or Metasomatic	Magmatic or Metasomatic	Magmatic or Metasomatic	Magmatic or Metasomatic	Magmatic or Metasomatic	Magmatic	Magmatic	Magmatic	Magmatic	Magmatic
No.	10	11	12	13	14	15	16	17	18	19	20
SiO_2	63.62	60.82	63.44	62.35	61.83	62.25	63.39	61.86	64.94	64.12	64.22
TiO_2	1.87	0.69	2.92	5.86	0.69	1.56	0.64	1.22	1.59	0.83	0.88
Al_2O_3	0.03	*bdl*	*bdl*	0.02	*bdl*	*bdl*	0.03	0.01	*bdl*	0.15	0.06
FeO	*bdl*	*bdl*	0.01	0.07	*bdl*	*bdl*	0.22	0.30	0.26	0.31	0.19
MnO	-	-	-	-	*bdl*	*bdl*	0.05	*bdl*	0.06	*bdl*	*bdl*
MgO	-	-	-	-	*bdl*	*bdl*	*bdl*	0.08	*bdl*	*bdl*	0.05
CaO	0.02	0.03	*bdl*	*bdl*	*bdl*	*bdl*	0.04	*bdl*	0.03	*bdl*	*bdl*
Na_2O	0.11	0.03	*bdl*	0.10	*bdl*	*bdl*	0.04	*bdl*	0.09	*bdl*	*bdl*
K_2O	14.99	15.41	16.75	16.68	15.15	15.65	15.93	16.64	14.08	15.80	16.36
ZrO_2	21.50	22.16	16.68	14.84	20.60	19.13	19.49	18.83	19.13	20.17	19.68
HfO_2	-	-	-	-	*bdl*	*bdl*	-	-	-	-	-
BaO	*bdl*	*bdl*	*bdl*	*bdl*	*bdl*	*bdl*	0.08	0.03	0.11	0.04	0.03
P_2O_5	-	-	-	-	*bdl*	*bdl*	0.10	0.12	*bdl*	*bdl*	*bdl*
La_2O_3	-	-	-	-	*bdl*	*bdl*	-	-	-	-	-
Ce_2O_3	-	-	-	-	*bdl*	*bdl*	-	-	-	-	-
Nb_2O_5	-	-	-	-	*bdl*	0.60	-	-	-	-	-
Total	**102.14**	**99.14**	**99.79**	**99.92**	**98.27**	**99.19**	**100.01**	**99.09**	**100.29**	**101.42**	**101.47**
Si	5.94	5.92	6.01	5.89	6.00	5.98	6.04	5.98	6.08	6.02	6.03
Ti	0.13	0.05	0.21	0.42	0.05	0.11	0.05	0.09	0.11	0.06	0.06
Al	0.00	*bdl*	*bdl*	0.00	*bdl*	*bdl*	0.00	0.00	*bdl*	0.02	0.01
Fe	*bdl*	*bdl*	0.00	0.01	*bdl*	*bdl*	0.02	0.02	0.02	0.02	0.01
Mn	-	-	-	-	*bdl*	*bdl*	0.00	*bdl*	0.00	*bdl*	*bdl*
Mg	-	-	-	-	*bdl*	*bdl*	*bdl*	0.01	*bdl*	*bdl*	0.01
Ca	0.00	0.00	*bdl*	-	*bdl*	*bdl*	0.00	*bdl*	0.00	*bdl*	*bdl*
Na	0.02	0.01	*bdl*	0.02	*bdl*	*bdl*	0.01	*bdl*	0.02	*bdl*	*bdl*
K	1.78	1.91	2.03	2.01	1.88	1.92	1.94	2.05	1.68	1.89	1.96
Zr	0.98	1.05	0.77	0.68	0.98	0.90	0.91	0.89	0.87	0.92	0.90
Hf	-	-	-	-	*bdl*	*bdl*	-	-	-	-	-
Ba	*bdl*	*bdl*	*bdl*	*bdl*	*bdl*	*bdl*	0.00	0.00	0.00	0.00	0.00
P	-	-	-	-	*bdl*	*bdl*	0.01	0.01	*bdl*	*bdl*	*bdl*
La	-	-	-	-	*bdl*	*bdl*	-	-	-	-	-
Ce	-	-	-	-	*bdl*	*bdl*	-	-	-	-	-
Nb	-	-	-	-	*bdl*	0.03	-	-	-	-	-
Sum	**8.85**	**8.94**	**9.02**	**9.03**	**8.91**	**8.93**	**8.97**	**9.05**	**8.79**	**8.94**	**8.98**
K_{alk}	20.34	21.48	22.51	22.48	21.07	21.47	21.71	22.65	19.34	21.16	21.80

Table 1 continued

Location	**Sunnfjord**	**Sunnfjord**	**Sunnfjord**	**Sunnfjord**	**Sunnfjord**	**Cancarix**	**Cancarix**	**Cancarix**	**Cancarix**	**Cancarix**	**Cancarix**
Group	2	**2**	**2**	**2**	**2**	**2**	**2**	**2**	**2**	**2**	**2**
Host rock	Syenite dyke	Syenite dyke	Syenite dyke	Syenite dyke	Syenite dyke	Lamproite	Lamproite	Lamproite	Lamproite	Lamproite	Lamproite
Suggested origin	Magmatic	Magmatic	Magmatic	Magmatic	Magmatic	Magmatic	Magmatic	Magmatic	Magmatic	Magmatic	Magmatic
No.	21	22	23	24	25	26	27	28	29	30	31
SiO_2	62.75	62.25	62.53	62.58	62.04	62.60	62.45	62.65	62.95	62.65	63.00
TiO_2	1.08	1.54	1.21	1.61	1.71	1.25	1.10	1.10	0.75	1.15	0.85
Al_2O_3	0.01	0.13	0.12	0.07	0.03	0.10	0.10	0.10	0.05	0.05	0.05
FeO	0.60	0.31	0.19	0.15	0.28	0.18	0.18	0.18	0.18	0.09	0.18
MnO	0.04	0.05	*bdl*	*bdl*	0.03	*bdl*	-	-	-	-	-
MgO	0.65	0.10	0.08	0.02	0.06	*bdl*	*bdl*	-	0.05	*bdl*	0.05
CaO	0.04	0.04	0.06	*bdl*	0.02	*bdl*	-	-	-	-	-
Na_2O	*bdl*	0.19	*bdl*	*bdl*	0.07	0.15	0.15	0.15	0.10	0.15	0.15
K_2O	15.79	15.33	15.98	16.17	13.93	15.75	16.10	16.10	15.95	16.25	16.10
ZrO_2	18.29	19.22	18.46	20.23	20.16	19.10	19.20	19.35	19.40	19.60	19.70
HfO_2	-	-	-	-	-	-	-	-	-	-	-
BaO	*bdl*	0.19	0.21	0.20	0.22	0.45	0.30	0.40	0.15	0.25	0.35
P_2O_5	0.04	0.10	*bdl*	*bdl*	*bdl*	-	-	-	-	-	-
La_2O_3	-	-	-	-	-	-	-	-	-	-	-
Ce_2O_3	-	-	-	-	-	-	-	-	-	-	-
Nb_2O_5	-	-	-	-	-	-	-	-	-	-	-
Total	**99.29**	**99.45**	**98.84**	**101.03**	**98.55**	**99.58**	**99.58**	**100.03**	**99.58**	**100.19**	**100.43**
Si	6.01	5.97	6.02	5.94	5.97	6.00	6.00	6.00	6.02	5.99	6.00
Ti	0.08	0.11	0.09	0.11	0.12	0.09	0.08	0.08	0.05	0.09	0.06
Al	0.00	0.01	0.01	0.01	0.00	0.01	0.01	0.01	0.01	0.01	0.01
Fe	0.05	0.02	0.02	0.01	0.02	0.02	0.02	0.02	0.02	0.02	0.02
Mn	0.00	0.00	*bdl*	*bdl*	0.00	*bdl*	-	-	-	-	-
Mg	0.09	0.01	0.01	0.00	0.01	*bdl*	*bdl*	-	0.01	*bdl*	0.01
Ca	0.00	0.00	0.01	*bdl*	0.00	*bdl*	-	-	-	-	-
Na	*bdl*	0.04	*bdl*	*bdl*	0.01	0.03	0.03	0.03	0.02	0.03	0.03
K	1.93	1.87	1.96	1.96	1.71	1.93	1.97	1.97	1.95	1.99	1.96
Zr	0.85	0.90	0.87	0.94	0.95	0.90	0.90	0.91	0.91	0.91	0.91
Hf	-	-	-	-	-	-	-	-	-	-	-
Ba	*bdl*	0.01	0.01	0.01	0.01	0.02	0.01	0.02	0.01	0.01	0.01
P	0.00	0.01	0.00	*bdl*	*bdl*	-	-	-	-	-	-
La	-	-	-	-	-	-	-	-	-	-	-
Ce	-	-	-	-	-	-	-	-	-	-	-
Nb	-	-	-	-	-	-	-	-	-	-	-
Sum	**9.02**	**8.96**	**9.00**	**8.98**	**8.82**	**8.99**	**9.02**	**9.01**	**8.99**	**9.02**	**9.01**
K_{alk}	21.42	21.29	21.78	21.80	19.55	21.83	22.20	22.17	21.89	22.28	22.06

Table 2 Average detection limits and errors for Terceira dalyite analyses

	Detection limit (wt. %)	Oxide error (wt. %)	Formula error (apfu)
SiO_2	0.034	0.326	0.045
TiO_2	0.038	0.054	0.004
Al_2O_3	0.020	0.027	0.003
Cr_2O_3	0.023	bdl	bdl
FeO	0.038	0.052	0.004
MnO	0.022	0.030	0.002
MgO	0.020	0.024	0.003
CaO	0.024	bdl	bdl
Na_2O	0.046	0.078	0.015
K_2O	0.021	0.199	0.026
ZrO_2	0.062	0.524	0.025
HfO_2	0.032	0.055	0.002
BaO	0.045	0.073	0.003
Total		0.661	

bdl = all values below detection limit

Table 3 Comparison of experimental and calculated lattice parameters

Lattice parameter	Experimental	Calculated	% difference
a/Å	7.371	7.211	-2.17
b/Å	7.730	7.679	-0.66
c/Å	6.912	6.787	-1.80
β/degrees	106.23	104.82	-1.33

Table 4 Whole rock major element analyses of the CCI syenite ejecta

Sample	**TER 30-1**	**TER 35-1**	**TER 30-6**	**TER 30-7**
SiO_2	64.14	64.78	63.90	64.80
TiO_2	0.58	0.45	0.61	0.41
Al_2O_3	15.76	15.51	15.82	16.18
Fe_2O_3	5.34	5.29	5.57	4.53
MnO	0.21	0.20	0.22	0.17
MgO	0.36	0.27	0.36	0.27
CaO	0.82	0.44	0.76	0.54
Na_2O	7.44	7.41	7.36	7.25
K_2O	4.93	5.11	4.98	5.10
P_2O_5	0.08	0.06	0.07	0.05
LOI	0.10	0.30	0.10	0.40
Total	99.76	99.82	99.75	99.70
A.I.	1.12	1.14	1.11	1.08
Na_2O/K_2O	1.51	1.45	1.48	1.42
CIPW				
Q	1.52	3.33	1.00	2.42
Or	29.25	30.32	29.55	30.14
Ab	53.76	51.58	53.84	54.83
An	0.00	0.00	0.00	0.00
Di	3.08	1.57	2.88	2.06
Hy	4.40	5.05	4.54	5.55
Ac	6.02	5.64	6.10	2.05
Il	1.10	0.85	1.16	0.78
Ap	0.19	0.14	0.16	0.12
NaS	0.61	1.18	0.41	0.97

Table 5 Electron microprobe analyses of dalyite from CCI syenite ejecta

Sample	**TER 30-1**	**TER 30-1**	**TER 30-1**	**TER 30-1**	**TER 30-1**	**TER 30-7**	**TER 30-7**	**TER 30-7**	**TER 30-7**	**TER 30-7**	**TER 30-7**	**TER 30-7**
Group	1	1	1	1	1	1	1	1	1	1	1	1
Suggested origin	Magmatic	Magmatic	Magmatic	Magmatic	Magmatic	Magmatic	Magmatic	Magmatic	Magmatic	Magmatic	Magmatic	Magmatic
SiO_2	62.9	62.6	62.4	62.2	62.4	62.9	63.0	62.4	62.6	62.6	63.0	63.0
TiO_2	0.10	0.23	0.19	0.13	0.11	0.17	0.10	0.12	0.41	0.09	0.06	0.27
Al_2O_3	*bdl*	*bdl*	0.03	0.03	*bdl*	*bdl*	0.04	0.04	0.05	0.03	*bdl*	*bdl*
Cr_2O_3	*bdl*	*bdl*	*bdl*	*bdl*	*bdl*	*bdl*	*bdl*	*bdl*	*bdl*	*bdl*	*bdl*	*bdl*
FeO	*bdl*	0.06	*bdl*	0.06	0.09	*bdl*	0.07	0.07	0.11	0.05	0.06	*bdl*
MnO	*bdl*	0.03	*bdl*	*bdl*	*bdl*	*bdl*	*bdl*	0.04	*bdl*	*bdl*	*bdl*	*bdl*
MgO	*bdl*	*bdl*	*bdl*	*bdl*	*bdl*	*bdl*	*bdl*	*bdl*	0.03	*bdl*	*bdl*	*bdl*
CaO	*bdl*	*bdl*	*bdl*	*bdl*	*bdl*	*bdl*	*bdl*	*bdl*	*bdl*	*bdl*	*bdl*	*bdl*
Na_2O	0.99	0.95	0.99	1.00	0.90	0.90	0.67	0.71	0.67	0.72	0.66	0.66
K_2O	14.6	15.0	14.9	14.8	14.7	14.8	15.0	15.0	15.0	15.2	15.3	15.1
ZrO_2	20.0	20.5	19.8	20.4	20.4	20.4	19.7	20.3	19.1	20.0	20.6	20.2
HfO_2	0.46	0.40	0.38	0.40	0.39	0.45	0.39	0.39	0.42	0.42	0.48	0.38
BaO	0.06	0.06	0.08	*bdl*	*bdl*	0.05	0.08	*bdl*	*bdl*	*bdl*	*bdl*	*bdl*
Total	**99.08**	**99.78**	**98.81**	**98.89**	**98.98**	**99.72**	**98.99**	**99.05**	**98.33**	**99.01**	**100.17**	**99.57**
Si	6.05	6.01	6.03	6.01	6.02	6.03	6.06	6.02	6.05	6.04	6.02	6.04
Ti	0.007	0.016	0.013	0.009	0.008	0.012	0.008	0.009	0.030	0.006	0.004	0.019
Al	*bdl*	*bdl*	0.004	0.003	*bdl*	*bdl*	0.005	0.004	0.006	0.004	*bdl*	*bdl*
Cr	*bdl*	*bdl*	*bdl*	*bdl*	*bdl*	*bdl*	*bdl*	*bdl*	*bdl*	*bdl*	*bdl*	*bdl*
Fe	*bdl*	0.005	*bdl*	0.004	0.007	*bdl*	0.005	0.006	0.009	0.004	0.005	*bdl*
Mn	*bdl*	0.002	*bdl*	*bdl*	*bdl*	*bdl*	*bdl*	0.004	*bdl*	*bdl*	*bdl*	*bdl*
Mg	*bdl*	*bdl*	*bdl*	*bdl*	*bdl*	*bdl*	*bdl*	*bdl*	0.004	*bdl*	*bdl*	*bdl*
Ca	*bdl*	*bdl*	*bdl*	*bdl*	*bdl*	*bdl*	*bdl*	*bdl*	*bdl*	*bdl*	*bdl*	*bdl*
Na	0.18	0.18	0.18	0.19	0.17	0.17	0.13	0.13	0.13	0.13	0.12	0.12
K	1.79	1.84	1.83	1.82	1.81	1.81	1.84	1.85	1.85	1.87	1.87	1.85
Zr	0.94	0.96	0.93	0.96	0.96	0.95	0.92	0.96	0.90	0.94	0.96	0.94
Hf	0.013	0.011	0.010	0.011	0.011	0.012	0.011	0.011	0.011	0.012	0.013	0.010
Ba	0.002	0.002	0.003	*bdl*	*bdl*	0.002	0.003	*bdl*	*bdl*	*bdl*	*bdl*	*bdl*
Sum	**8.982**	**9.026**	**9.000**	**9.007**	**8.986**	**8.986**	**8.982**	**8.994**	**8.990**	**9.006**	**8.992**	**8.979**
K_{alk}	21.98	22.34	22.39	22.32	22.06	21.99	21.90	22.03	21.98	22.27	22.13	21.94

Table 6 Results of computer modelling undertaken using the GULP code (Gale, 1997)

Substitution	Solution scheme	E_{sol} (eV)
Ti → Zr	$TiO_2 + Zr_{Zr} \rightarrow Ti_{Zr} + ZrO_2$	-0.25
Ti → Si	$TiO_2 + Si_{Si} \rightarrow Ti_{Si} + SiO_2$	-0.98
Ti → K	$TiO_2 + 4K_K \rightarrow Ti_K^{\bullet\bullet\bullet} + 3V_K' + 2K_2O$	30.64
Hf → Zr	$HfO_2 + Zr_{Zr} \rightarrow Hf_{Zr} + ZrO_2$	-0.31
Hf → Si	$HfO_2 + Si_{Si} \rightarrow Hf_{Si} + SiO_2$	2.67
Hf → K	$HfO_2 + 4K_K \rightarrow Hf_K^{\bullet\bullet\bullet} + 3V_K' + 2K_2O$	29.09
Fe^{2+} → Zr	$FeO + Zr_{Zr} \rightarrow Fe_{Zr}'' + V_O^{\bullet\bullet} + ZrO_2$	12.52
Fe^{2+} → Si	$FeO + Si_{Si} \rightarrow Fe_{Si}'' + V_O^{\bullet\bullet} + SiO_2$	13.69
Fe^{2+} → K	$FeO + K_K \rightarrow Fe_K^{\bullet} + V_K' + K_2O$	8.86
Mg^{2+} → Zr	$MgO + Zr_{Zr} \rightarrow Mg_{Zr}'' + V_O^{\bullet\bullet} + ZrO_2$	12.97
Mg^{2+} → Si	$MgO + Si_{Si} \rightarrow Mg_{Si}''+ V_O^{\bullet\bullet} + SiO_2$	14.07
Mg^{2+} → K	$MgO + K_K \rightarrow Mg_K^{\bullet} + V_K' + K_2O$	9.61
Ba^{2+} → Zr	$BaO + Zr_{Zr} \rightarrow Ba_{Zr}'' + V_O^{\bullet\bullet} + ZrO_2$	12.54
Ba^{2+} → Si	$BaO + Si_{Si} \rightarrow Ba_{Si}''+ V_O^{\bullet\bullet} + SiO_2$	16.58
Ba^{2+} → K	$BaO + K_K \rightarrow Ba_K^{\bullet} + V_K' + K_2O$	4.94